Journal Name

ARTICLE

On the Phase Control of $CuInS_2$ Nanoparticles from Cu-/In-Xanthates

Received 00th January 20xx,
Accepted 00th January 20xx

DOI: 10.1039/x0xx00000x

www.rsc.org/

Mundher Al-Shakban,[a] Peter D Matthews,[c] Xiang L. Zhong,[a] Inigo Vitorica-Yrezabal,[b] James Raftery,[b] David J. Lewis[a] and Paul O'Brien*[a,b]

In this paper we report the synthesis and single-crystal X-ray characterisation of six novel indium(III) xanthate complexes. These xanthates have been used as an In-source for the synthesis of highly crystalline $CuInS_2$ nanoparticles in conjunction with a Cu(I)-xanthate. In synthesising the nanoparticles we have also demonstrated an ability to control the phase of the material through choice of solvent.

Introduction

Transition metal chalcogenides (TMCs) have witnessed a remarkable surge in interest in recent years, owing to extensive investigations into their exciting properties and wide ranging applications. These applications, which include playing key roles in sensors, photovoltaics, photocatalysts and other electronics, are driven by the presence of a controllable band gap which causes the semi-conductor properties of TMCs.[1–3]

I-III-VI_2 ternary TMCs, such as $CuInS_2$ (CIS), offer an environmentally benign alternative to the more common II-VI binary systems like PbS or CdS.[4] CIS has been explored as the active light harvesting component in photovoltaic devices[5–7] as it has a direct band gap of 1.5 eV, an absorption coefficient $>10^5$ cm^{-1} and a good defect tolerance.[8–10] However, it is synthetically challenging to make pure CIS owing to the difference in reactivity of Cu(I) (soft Lewis acid) and In(III) (hard Lewis acid) to sulfur. Additionally, the phase diagram of $CuInS_2$ is complex, and the window to form $CuInS_2$ at temperatures lower than 800 °C is narrow.[11] These challenges mean that the formation of contaminating Cu_xS_y phases is often observed.[12]

The challenge that we address in this manuscript is one of how to reliably and easily synthesise $CuInS_2$, whilst demonstrating a certain level of control. In order to do this, we turned to a combination of copper(I) xanthates[13] and novel indium(III) xanthates. Metal xanthates $[M(S_2COR)_x]$ have been shown to be excellent precursors to an array of metal chalcogenides previously, including complex materials such as alkaline earth metal sulfides.[14–26] The xanthates breakdown cleanly to form metal sulfides via a Chugaev elimination mechanism, in which volatile gases are the only by-products.[27]

Previous synthetic routes to CIS nanoparticles have included the reaction of metal salts (e.g. CuI, CuOAc, $In(OAc)_3$ or indium stearate) with thiols/elemental sulfur,[28–32] cation exchange of Cu^+ for In^{3+} into previously prepared Cu_xS_y nanoparticles,[33–35] or the use of single source precursors like $[(PPh_3)_2CuIn(SEt)_4]$,[36] thiobenzoates,[37] and $[(Ph_3P)_2Cu\text{-}(\mu\text{-}SEt)_2In(SEt)_2]$.[38] However, these procedures are relatively complex, requiring fine control of the reaction conditions. Additionally, there have been some reports of the use of simple, previously known xanthates to make CIS.[39–41] Here we present a robust synthetic route which demonstrates control over the phase of the obtained CIS through choice of the reaction solvent.

Results and Discussion

Precursors

We report here the synthesis and single crystal structures of six novel indium xanthates: $[In(S_2CO^nPr)_3]$ (**8**), $[In(S_2CO^iBu)_3]$ (**10**), $[In(S_2CO(CH_2)_2OEt)_3]$ (**11**), $[In(S_2CO(CH_2)_2OMe)_3]$ (**12**) $[In(S_2CO(CH_2)_2C(OMe)(Me)_2)_3]$ (**13**) and $[In(S_2COC(H)(Me)CH_2OMe)_3]$ (**14**) as well as $[K(S_2CO(CH_2)_2C(OMe)(Me)_2)]$ (ESI Tables S2 and S3). We also prepared $[In(S_2CO^iPr)_3]$ (**9**), which has previously been reported.[42] These complexes were prepared from the reaction of a previously prepared potassium xanthate (from the insertion of CS_2 into the relevant potassium alkoxide) and indium(III) chloride. Crystals suitable for X-ray analysis can be grown from the slow evaporation of chloroform at room temperature.

Compounds **8**, **11**, **12** and **13** adopt a monoclinic crystal system with space groups $P2_1/c1$, $C2/c$, $P21/n$, and $P21/n$ respectively, whilst **10** is orthorhombic $Pbca$ and **14** is trigonal R-3.

[a] School of Materials, University of Manchester, Oxford Road, Manchester, M13 9PL (UK). E-mail: paul.obrien@manchester.ac.uk
[b] School of Chemistry, University of Manchester, Oxford Road, Manchester, M13 9PL (UK).
[c] Lennard-Jones Laboratories, School of Chemical and Physical Sciences, Keele University, Keele, Borough of Newcastle-under-Lyme, Staffordshire ST5 5BG, UK

† Electronic Supplementary Information (ESI) available: TGA analysis, single crystal X-ray crystallography, UV-vis and NMR data. Crystallographic data is available from the CCDC: 1812198-1812204. See DOI: 10.1039/x0xx00000x

In all cases the central In ions are 6-coordinate, bound by three chelating xanthate ligands in a distorted octahedral manner (Figure 1). The In-S bond lengths show little variation across the series: 2.5650(8)-2.6166(8) Å (**8**), 2.575(1)-2.626(1) Å (**10**), 2.5577(9)-2.655(1) Å (**11**), 2.5683(6)-2.6298(6) Å (**12**), 2.558(2)-2.634(2) Å (**13**) and 2.576(2)-2.63(2) Å (**14**). This is also mirrored in the S-In-S bond angles of 69.93(2)-70.51(3)° (**8**), 69.68(3)-70.27(3)° (**10**), 69.71(3)-70.30(3)° (**11**), 70.06(2)-70.44(2)° (**12**), 69.72(6)-70.03(5)° (**13**) and 69.66(3)° (**14**) and S-C-S bond angles of the xanthates: 122.0(2)-122.2(2)° (**8**), 121.3(2)-122.4(3)° (**10**), 122.1(2)-123.2(2)° (**11**), 121.8(1)-122.4(1)° (**12**), 121.4(4)-123.0(4)° (**13**) and 121.9(3)° (**14**).

It is clear from the bond angles, that the distortion around the In centre, noted above, is due to the sharp ligand bite angle and associated formation of a CS_2In 4-membered chelate ring. This results in an acute S-In-S intraligand bond angle, in turn forcing the S-In-S interligand bond angle to become obtuse.

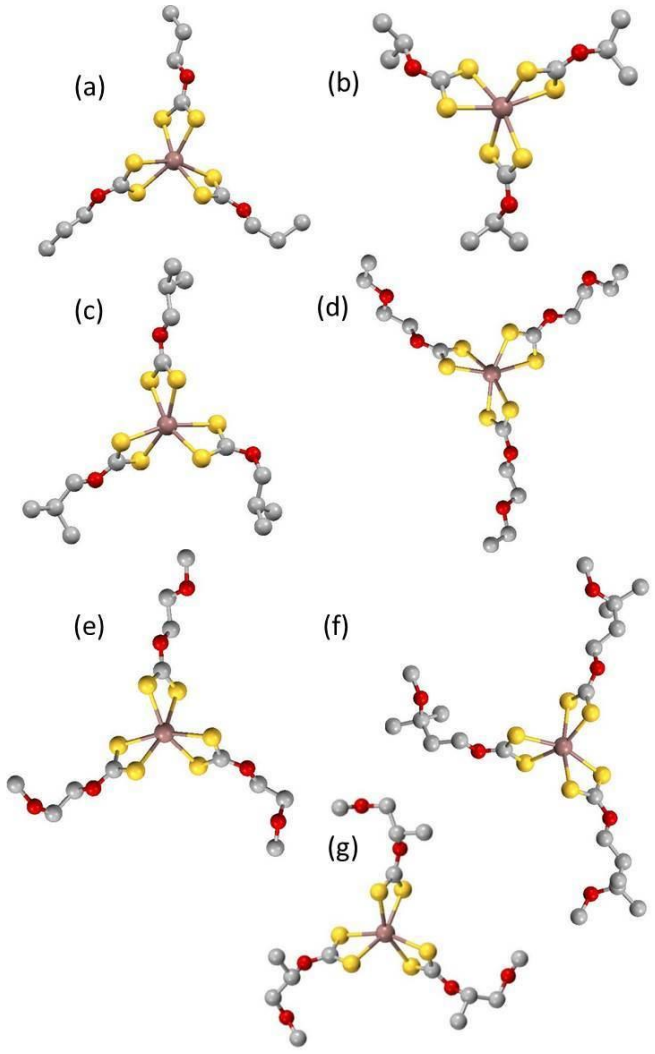

Figure 1. The structures of the indium xanthates. (a) $[In(S_2CO^nPr)_3]$ (**8**), (b) $[In(S_2CO^iPr)_3]$ (**9**),[42] (c) $[In(S_2CO^iBu)_3]$ (**10**), (d), $[In(S_2CO(CH_2)_2OEt)_3]$ (**11**), (e) $[In(S_2CO(CH_2)_2OMe)_3]$ (**12**), (f) $[In(S_2CO(CH_2)_2C(OMe)(Me)_2)_3]$ (**13**) and (g) $[In(S_2COC(H)(Me)CH_2OMe)_3]$ (**14**). H atoms are omitted for clarity. Bronze = In, yellow = S, red = O, grey = C.

The decomposition of the indium complexes was assessed via thermogravimetric analysis (TGA, ESI Figure S1). Complexes **8**-**10**, i.e. those with a pure hydrocarbon xanthate backbone, decompose cleanly in one-step to form InS at 120-150 °C. In contrast, **11**-**14**, which have an ether moiety within the xanthate chain undergo a two-step process, initially forming In_2S_3 before the remaining sulfur is driven off to leave InS.

Synthesis of Nanoparticles

We initially chose complex **11,** $[In(S_2CO(CH_2)_2OEt)_3]$, as our source of In, reasoning that the two-step decomposition process would give rise to a control handle for the phase produced. We selected triphenylphosphine copper(I) 2-ethoxyethylxanthate (**15**)[13] as the copper source to avoid any potential problems involving ligand exchange.

We prepared $CuInS_2$ nanoparticles using the hot-injection method in two distinct solvent systems. Firstly, we suspended a 1:1 ratio of **11**:**15** in octadecene and injected it into castor oil preheated to 260 °C. This resulted in the formation of hexagonal phase $CuInS_2$ (Figures 2a and 2b), with unit cells comparable to the literature (ESI Table S4).[43]

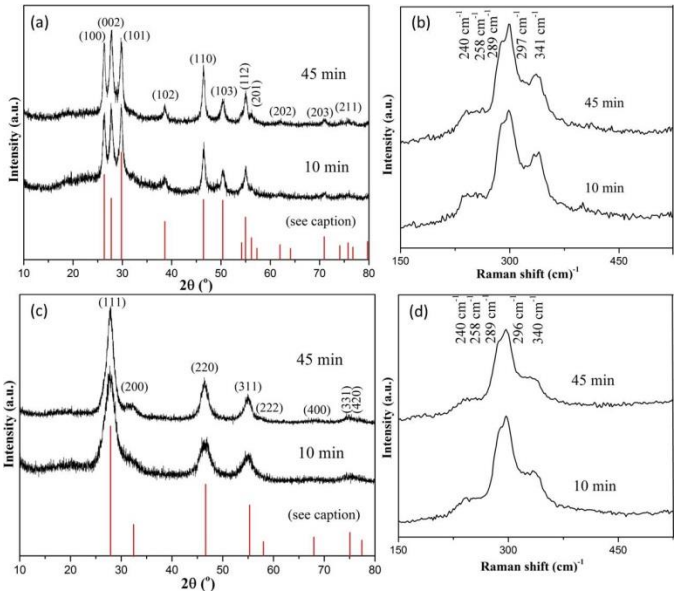

Figure 2. The pXRD patterns and Raman spectra of CIS prepared at 260 °C via hot injection, (a, b) hexagonal CIS and (c, d) cubic CIS. In each case the upper pattern corresponds to a 45 minute reaction, whilst the lower corresponds to a 10 minute reaction length. Hexagonal CIS reference pattern generated from Qi *et al.*,[43] cubic CIS reference pattern generated from Pan *et al.*[44]

Secondly, we dissolved the precursors **11** and **15** in separate mixtures of trioctylphosphine (1 ml) and oleylamine (1 ml). These two solutions were then injected into oleylamine (20 ml) that had been preheated to 260 °C and held at that temperature for a set length of time before quenching. This resulted in the formation of cubic CIS (i.e. zincblende structure) again with unit cells comparable to the literature (Figures 2c and 2d and ESI Table S4).[44]

This intriguing result indicates that the choice of solvent has a remarkable impact on the phase that is formed. Octadecene is of course a non-coordinating solvent, but the main

component of castor oil is the triester of glycerol and ricinoleic acid, which does have pendant hydroxyl groups on the backbone and has been previously used as a 'green' capping ligand.[45–47] Oleylamine and trioctylphosphine on the other hand are very much coordinating ligands that can act to stabilise metal surfaces.[48] It is interesting to note that in a previous study oleic acid (i.e. an acid capping ligand) gave the cubic, zincblende structure, which is the reverse of what we observe here.[44] On the other hand, a reaction (of different precursors) in oleylamine gave the same cubic CIS that we report.[49]

In order to be sure that there was no exchange of the alkoxy group of the xanthates for oleylamine (to make a dithiocarbamate) we heated a solution of **11** in oleylamine to 100 °C (i.e. just below the initial breakdown temperature) and then ran a ^{1}H NMR of the resulting mixture (ESI Figures S8 and S9). For **11** + oleylamine, there was no evidence of any exchange occurring with the oleylamine signals remaining identical after heating (ESI Figure S8). There is some slight shifting of the xanthate signals after heating (ESI Figure S9) but this is most likely due to the beginnings of decomposition. We have previously conducted a similar experiment for **15** and seen no ligand exchange either.[13]

Figures 2b and 2d show the Raman spectra of $CuInS_2$ nanoparticles. 240 (E mode), 258 (E/B_2 modes), 289 (A_1 mode), 297 (likely associated with lattice ordering) and 341 (B_2 mode) cm^{-1}.[50–53] Similar peak positions were observed for both hexagonal and cubic CIS with a slight shift for some individual peaks.

The particles themselves are highly crystalline, though of an indeterminate shape for both solvent systems (Figure 3). Lattice fringes for hexagonal $CuInS_2$ can be indexed to the (100) plane (Figure 3b), and for cubic $CuInS_2$ can be indexed to the (111) plane. There is little discernible difference from a 10 min reaction (Figure 3) and a 45 min reaction (ESI Figure S4)

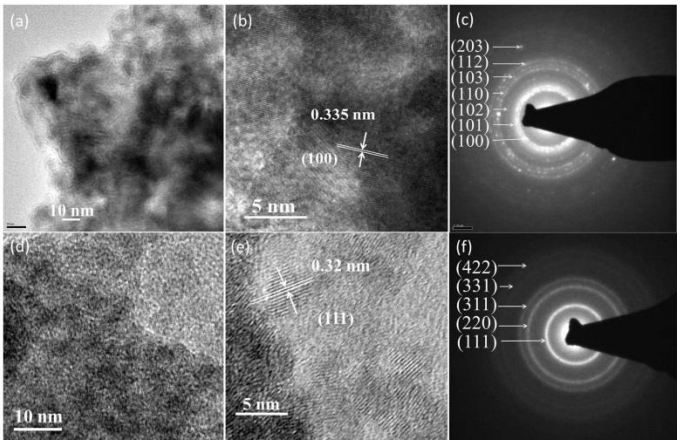

Figure 3. TEM images and associated selected area electron diffraction (SAED) patterns for (a)-(c) hexagonal $CuInS_2$ from a 10 min reaction and (d)-(f) cubic $CuInS_2$ from a 10 min reaction.

Energy dispersive x-ray spectroscopy (EDX) indicates that the composition of the particles is consistent across the different solvent systems and reaction times (ESI Table S5, Figure S3), close to the ideal $CuInS_2$ ratios. Raman spectroscopy gave additional confirmation as to the purity of the phases We have also measured the optical properties of the nanoparticles and found them to be in the range 1.47-1.53 eV, but all within error of each other (ESI Figure S7, Table S6). This result is consistent with the literature.[44,54]

In order to confirm the consistency of the phase control, we also performed the experiment using the equivalent 2-methoxyethylxanthate (i.e. **12** and the corresponding copper(I) analogue). We found that the precursors behaved identically as **11** and **15** (ESI Figures S5-S6).

Conclusions

We have demonstrated an ability to generate highly crystalline $CuInS_2$ from indium and copper xanthate precursors, whilst exhibiting phase control through choice of solvent. We have reported the crystal structures of six novel indium xanthates, comprehensively extending this family of compounds.

Experimental

Materials and Synthesis: All chemicals were purchased from Sigma Aldrich, and were used as received. Elemental analyses (EA) and Thermogravimetric analyses (TGA) were carried out by the Microelemental Analysis service at the University of Manchester. EA was performed using a Flash 2000 Thermo Scientific elemental analyzer and TGA data was obtained with Mettler Toledo TGA/DSC1 star^e system between the range of 30 - 600 °C at a heating rate of 10 °C min^{-1} under nitrogen flow. NMR spectra were recorded in $CDCl_3$ and D_2O solutions on a Bruker Ascend spectrometer operating at 400 MHz. Transmission electron microscope (TEM) images were collected using an FEI Tecnai G2 F30 with Schottky Field Emitter operated at 300keV. Powder X-ray diffraction (pXRD) analyses were carried out using an X-Pert diffractometer with a Cu-$K_{\alpha1}$ source (λ = 1.54059 Å), the samples were scanned between 10 and 80°, the applied voltage was 40 kV and the current 30 mA. Raman spectra were measured using a Renishaw 1000 Micro-Raman System equipped with a 514 nm laser. UV-Vis spectra were collected on a Shimadzu UV-1800, using 3.09 mM solution of $CuInS_2$ nanoparticles in methanol. Potassium *iso*-butylxanthate (**3**), Potassium 2-methoxyethylxanthate (**4**), potassium 2-ethoxyethylxanthate (**5**), potassium 3-methoxy-3-methyl-1-butylxanthate (**6**) potassium 1-methoxy-2-propylxanthate (**7**) and triphenylphosphine copper(I) 2-ethoxyethylxanthate (**15**) were all prepared according to our previously published procedure.[13]

Synthesis of potassium *n*-propylxanthate (1): Potassium *n*-propylxanthate was prepared following a literature method.[55] Potassium hydroxide (11.2 g, 0.20 mol) and *n*-propanol (150 ml) were stirred for 2 h at room temperature and then CS_2 (15.2 g, 12.0 ml, 0.20 mol) was added dropwise to the reaction, resulting in an orange solution. The unreacted

alcohol was removed *in vacuo* and the yellow solid product was dried to give [K(S_2CO^nPr)] (27.3 g, 0.157 mol, 78.4% yield). M.p. = 228-230 °C. Calc. for $C_4H_7KOS_2$ (%):C 27.6, H 4.05, S 36.7, K 22.5; found: C 27.8, H 3.99, S 37.0, K 22.9. FT-IR (cm^{-1}): 2965 (m), 2937(w), 2873 (w), 1453 (m), 1445 (w), 1270 (m), 1148 (s), 1087 (s), 1061 (s), 925 (m), 902 (m), 765.0 (s), 660.1 (s), 544 (s). ^{1}H NMR (400 MHz, D_2O) δ (ppm) = 0.89 (t, 3H, C***H***$_3$), 1.68 (s, 2H, CH_2C***H***$_2CH_3$), 4.31 (t, 2H, OC***H***$_2CH_2$).

Synthesis of potassium *iso*-propylxanthate (2): [K(S_2CO^iPr)] was prepared via the same method as **1**, using *iso*-propanol (150 ml). (25.8 g, 0.148 mol, 74.1% yield). M.p. = 223-227 °C. Calc. for $C_4H_7KOS_2$ (%):C 27.6, H 4.05, S 36.7, K 22.5; found: C 27.6, H 3.96, S 36.6, K 23.3. FT-IR (cm^{-1}): 2970 (m), 1460 (w), 1370 (m), 1182 (m), 1048 (s), 901 (s), 1092 (s), 662 (w), 583 (w). ^{1}H NMR (400 MHz, D_2O) δ (ppm) = 1.25 (d, 6H, CH(C***H***$_3$)$_2$), 5.44 (s, 1H, C***H***$(CH_3)_2$).

Synthesis of indium(III) *n*-propylxanthate (8): A solution of potassium *n*-propylxanthate (2.35 g, 0.0135 mol) in water (60 ml) was added to a solution of $InCl_3$ (1.00 g, 0.0045 mol) in the same amount of water. A white precipitate was obtained after continuous stirring for 30 min at room temperature. The solid was collected by vacuum filtration and washed three times with water. The product was dried in *vacuo* and recrystallized from chloroform at room temperature to give (1.96 g, 0.0038 mol, 83.76% yield). M.p. = 102-104 °C. Calc. for $C_{12}H_{21}InO_3S_6$ (%): C 27.7, H 4.07, S 36.9, In 22.1; found: C 27.8, H 3.98, S 36.1, In 22.0. FT-IR (cm^{-1}): 2970 (m), 2875(w), 1453 (m) 1245 (s), 1217 (s), 1136 (m), 1039 (s), 1034 (s), 937.5 (m), 899.2 (w), 755.2 (m), 648.8 (m), 561.6 (w). ^{1}H NMR (400 MHz, $CDCl_3$) δ (ppm) = 1.06 (t, 3H, C***H***$_3$), 1.91 (s, 2H, CH_2C***H***$_2CH_3$), 4.43 (t, 2H, OC***H***$_2CH_2$).

Synthesis of indium(III) *iso*-propylxanthate (9): [In(S_2CO^iPr)$_3$] was synthesized via the same method as **8**, using potassium *iso*-propylxanthate (2.35 g, 0.0135 mol). (1.85 g, 0.0035 mol, 79.0% yield). M.p. = 142-144 °C. Calc. for $C_{12}H_{21}InO_3S_6$ (%): C 27.7, H 4.07, S 36.9, In 22.1; found: C 27.8, H 3.98, S 36.7, In 22.5. FT-IR (cm^{-1}): 2976 (m), 2930 (w), 1461 (m), 1373 (m), 1232 (s), 1142 (m), 1083 (s), 1011 (s), 899.3 (m), 808.4 (w), 645.2 (m), 567.7 (w). ^{1}H NMR (400 MHz, $CDCl_3$) δ (ppm) = 1.5 (d, 6H, CH(C***H***$_3$)$_2$), 5.14 (s, 1H, C***H***$(CH_3)_2$).

Synthesis of indium(III) *iso*-butylxanthate (10): [In(S_2CO^iBu)$_3$] was synthesized via the same method as **8**, using potassium *iso*- butylxanthate (2.54 g, 0.0135 mol). (1.94 g, 0.0034 mol, 76.7% yield). M.p. = 109-113 °C. Calc. for $C_{15}H_{27}InO_3S_6$ (%): C 32.0, H 4.84, S 34.1, In 20.4; found: C 32.0, H 4.79, S 34.1, In 20.2. FT-IR (cm^{-1}): 2955 (m), 2870 (w), 1466 (m), 1454 (m), 1372 (m), 1221 (s), 1197 (m), 1025 (s), 958.3 (s), 822.5 (w), 654.6 (m), 575.3 (w). ^{1}H NMR (400 MHz, $CDCl_3$) δ (ppm): 0.96 (d, 6H, CH(C***H***$_3$)$_2$), 2.12 (s, 1H, C***H***$(CH_3)_2$), 4.15 (d, 2H,OC***H***$_2$CH).

Synthesis of indium(III) 2-ethoxyethylxanthate (11): [In($S_2CO(CH_2)_2OEt$)$_3$] was synthesized via the same method as **8**, using potassium 2-ethoxyethylxanthate (2.75 g, 0.0135 mol). (2.25 g, 0.0037 mol, 82% yield). M.p. = 81-84 °C. Calc. for $C_{15}H_{27}InO_6S_6$ (%): C 29.5, H 4.46, S 31.5, In 18.8; found: C 29.5, H 4.36, S 31.2, In 18.7. FT-IR (cm^{-1}): 2971 (m), 2865 (w), 1441 (m), 1384 (m), 1352 (w), 1214 (s), 1116 (s), 1035 (s), 998.5 (s), 936.1 (m), 863.3 (m), 836.1 (m). ^{1}H NMR (400 MHz, $CDCl_3$) δ (ppm): 1.17 (t, 3H, OCH_2C***H***$_3$), 3.51 (q, 2H, OC***H***$_2CH_3$), 3.74 (t, 2H, CH_2C***H***$_2$O), 4.49(t, 2H, C***H***$_2CH_2$O).

Synthesis of indium(III) 2-methoxyethylxanthate (12): [In($S_2CO(CH_2)_2OMe$)$_3$] was synthesized via the same method as **8**, using potassium 2-methoxyethylxanthate (2.56 g, 0.0135 mol). (2.2 g, 0.0038 mol, 86.1% yield). M.p. = 95-98 °C. Calc. for $C_{12}H_{21}InO_6S_6$ (%): C 25.4, H 3.73, S 33.8, In 20.2; found: C 25.4, H 3.66, S 33.5, In 19.8. FT-IR (cm^{-1}): 2922 (m), 1438 (m), 1392 (m), 1367 (m), 1212 (s), 1120 (s) 1092 (s), 1036 (s), 1021 (s), 976.2 (s), 845.6 (s), 661.6 (m), 575.8 (w). ^{1}H NMR (400 MHz, $CDCl_3$) δ (ppm): 3.36 (s, 3H, OC***H***$_3$), 3.71 (t, 2H, CH_2C***H***$_2$O), 4.50 (t, 2H, C***H***$_2CH_2$O).

Synthesis of indium(III) 3-methoxy-3-methyl-1-butylxanthate (13): [In($S_2CO(CH_2)_2C(OMe)(Me)_2$)$_3$] was synthesized via the same method as **8**, using potassium 3-methoxy-3-methyl-1-butylxanthate (3.13 g, 0.0135 mol). (2.3 g, 0.0033 mol, 73.6% yield). M.p. = 78-81 °C. Calc. for $C_{21}H_{39}InO_6S_6$ (%): C 36.3, H 5.66, S 27.6, In 16.6; found: C 36.5, H 5.67, S 27.3, In 16.5. FT-IR (cm^{-1}): 2975 (m), 2825 (w), 1466 (m), 1381 (m), 1366 (m), 1310 (w), 1227 (s), 1210 (s), 1173 (s), 1155 (s), 1074 (s), 1040 (s), 1019 (s), 933.7 (m), 871.4 (m), 788.1 (w), 751.9 (m), 644.7 (w), 568.2 (w). ^{1}H NMR (400 MHz, $CDCl_3$) δ (ppm): 1.24 (s, 6H, $CH_2C(C$***H***$_3)_2OCH_3$), 2.09 (t, 2H, C***H***$_2C(CH_3)_2OCH_3$), 3.23 (s, 3H, $CH_2C(CH_3)_2OC$***H***$_3$), 4.59 (t, 2H, C***H***$_2CH_2C(CH_3)_2OCH_3$).

Synthesis of indium(III) 1-methoxy-2-propylxanthate (14): [In($S_2COC(H)(Me)CH_2OMe$)$_3$] was synthesized via the same method as **8**, using potassium 1-methoxy-2-propylxanthate (2.75 g, 0.0135 mol). (2.25 g, 0.0036 mol, 82% yield). M.p. = 109-112 °C. Calc. for $C_{15}H_{27}InO_6S_6$ (%): C 29.5, H 4.46, S 31.5, In 18.8; found: C 29.3, H 4.26, S 29.3, In 19.4. FT-IR (cm^{-1}): 2984 (m), 2938 (w), 1448 (m), 1392 (w), 1344(w), 1236 (s), 1198 (s), 1161 (m), 1121 (w), 1092 (w), 1055 (s), 1009 (s), 943.9 (m), 815.6 (m), 643.1 (w), 574.0 (w). ^{1}H NMR (400 MHz, $CDCl_3$) δ (ppm): 1.39 (d, 3H, CHC***H***$_3$), 3.35 (s, 3H, OC***H***$_3$), 3.50-3.59 (m, 2H, C***H***$_2$O), 5.08 (m, 1H, C***H***CH_3).

X-ray Crystallography: Single crystal X-ray diffraction was performed using a Bruker diffractometer with a Cu-K_α source (λ = 1.5418 Å) (**10**, **12**, **13**) and XtaLAB AFC11 (RINC): Kappa single diffractometer with a Mo-K_α source (λ = 0.71073 Å) (**6**, **8**, **14**) SuperNova, Single source at offset, Eos diffractometer with a Mo-K source (**11**). Crystallographic data available from the CCDC, numbers: 1812198-1812204.

Synthesis of $CuInS_2$ nanoparticles: $CuInS_2$ nanocrystals were synthesized via the hot injection method and a typical procedure is described. A stoichiometric mixture of **15** (0.0752 g, 0.0001 mol) and **11** (0.0609 g, 0.0001mol) were used. The reactions were performed under nitrogen. To obtain a

hexagonal phase, the mixture was suspended in octadecene (2 ml) and injected into 20 ml castrol oil preheated to 260 °C. To form a zinc blende $CuInS_2$, the precursors were dissolved into trioctylphosphine (1 ml) and oleylamine (1 ml) and injected into oleylamine (20 ml) preheated to 260 °C. After a set period of time (10 or 45 min), the solution was cooled to room temperature with the addition of *iso*-propanol and the particles separated by centrifugation. The nanoparticles were extracted by diluting the resultant product with 30ml methanol (three times) and 30ml acetone (two times).

Acknowledgements

The authors would like to acknowledge the Iraqi Culture Attaché in London for financial support (M.A.S.). Some of the equipment used in this study were provided by the EPSRC Core Capability in Chemistry grant EP/K039547/1. P.D.M. would like to acknowledge the UK Government and European Union as contributors to the Smart Energy Network Demonstrator, ERDF project number 32R16P00706).

Notes and references

1. P. D. Matthews, P. D. McNaughter, D. J. Lewis and P. O'Brien, *Chem. Sci.*, 2017, **8**, 4177–4187.
2. M. V. Kovalenko, L. Manna, A. Cabot, Z. Hens, D. V. Talapin, C. R. Kagan, V. I. Klimov, A. L. Rogach, P. Reiss, D. J. Milliron, P. Guyot-Sionnnest, G. Konstantatos, W. J. Parak, T. Hyeon, B. A. Korgel, C. B. Murray and W. Heiss, *ACS Nano*, 2015, **9**, 1012–1057.
3. A. A. Tedstone, D. J. Lewis and P. O'Brien, *Chem. Mater.*, 2016, **28**, 1965–1974.
4. A. D. P. Leach and J. E. Macdonald, *J. Phys. Chem. Lett.*, 2016, **7**, 572–583.
5. S. Wagner, J. L. Shay, P. Migliorato and H. M. Kasper, *Appl. Phys. Lett.*, 1974, **25**, 434–435.
6. L. L. Kazmerski and G. A. Sanborn, *J. Appl. Phys.*, 1977, **48**, 3178–3180.
7. L. L. Kazmerski, F. R. White and G. K. Morgan, *Appl. Phys. Lett.*, 1976, **29**, 268–270.
8. N. N. Syrbu, R. V Cretu and V. E. Tezlevan, *Cryst. Res. Technol.*, 1998, **33**, 135–144.
9. W. Yue, S. Han, R. Peng, W. Shen, H. Geng, F. Wu, S. Tao and M. Wang, *J. Mater. Chem.*, 2010, **20**, 7570–7578.
10. H. Y. Ueng and H. L. Hwang, *J. Phys. Chem. Solids*, 1989, **50**, 1297–1305.
11. J. J. M. Binsma, L. J. Giling and J. Bloem, *J. Cryst. Growth*, 1980, **50**, 429–436.
12. J. Kolny-Olesiak and H. Weller, *ACS Appl. Mater. Interfaces*, 2013, **5**, 12221–12237.
13. M. Al-Shakban, P. D. Matthews, G. Deogratias, P. D. McNaughter, J. Raftery, I. Vitorica-Yrezabal, E. B. Mubofu and P. O'Brien, *Inorg. Chem.*, 2017, **56**, 9247–9254.
14. M. Afzaal, C. L. Rosenberg, M. A. Malik, A. J. P. White and P. O'Brien, *New J. Chem.*, 2011, **35**, 2773–2780.
15. P. S. Nair, T. Radhakrishnan, N. Revaprasadu, G. A. Kolawole and P. O'Brien, *J. Mater. Chem.*, 2003, **22**, 3129–3135.
16. M. Afzaal, M. A. Malik and P. O'Brien, *J. Mater. Chem.*, 2010, **20**, 4031–4040.
17. E. A. Lewis, S. Haigh and P. O'Brien, *J. Mater. Chem. A*, 2014, **2**, 570–580.
18. E. A. Lewis, P. D. McNaughter, Z. Yin, Y. Chen, J. R. Brent, S. A. Saah, J. Raftery, J. A. M. Awudza, M. A. Malik, P. O'Brien and S. J. Haigh, *Chem. Mater.*, 2015, **27**, 2127–2136.
19. P. D. McNaughter, S. A. Saah, M. Akhtar, K. Abdulwahab, M. A. Malik, J. Raftery, J. A. M. Awudza and P. O'Brien, *Dalton Trans.*, 2016, **45**, 16345–16353.
20. P. D. Matthews, M. Akhtar, M. A. Malik, N. Revaprasadu and P. O'Brien, *Dalton Trans.*, 2016, **45**, 18803–18812.
21. N. Alam, M. S. Hill, G. Kociok-Köhn, M. Zeller, M. Mazhar and K. C. Molloy, *Chem. Mater.*, 2008, **20**, 6157–6162.
22. J. M. Clark, G. Kociok-Köhn, N. J. Harnett, M. S. Hill, R. Hill, K. C. Molloy, H. Saponia, D. Stanton and A. Sudlow, *Dalton Trans.*, 2011, **40**, 6893–6900.
23. M. Al-Shakban, P. D. Matthews, N. Savjani, X. L. Zhong, Y. Wang, M. Missous and P. O'Brien, *J. Mater. Sci.*, 2017, **52**, 12761–12771.
24. T. Rath, A. J. MacLachlan, M. D. Brown and S. A. Haque, *J. Mater. Chem. A*, 2015, **3**, 24155–24162.
25. M. Al-Shakban, P. D. Matthews and P. O'Brien, *Chem. Commun.*, 2017, **53**, 10058–10061.
26. S. H. Lu, T. F. Chen, A. J. Wang, D. Zheng, Y. L. Li and Y. S. Wang, *Mater. Sci. Eng. B*, 2016, **203**, 19–26.
27. M. A. Buckingham, A. L. Catherall, M. S. Hill, A. L. Johnson and J. D. Parish, *Cryst. Growth Des.*, 2017, **17**, 907–912.
28. Y. su Kim, Y. Lee, Y. Kim, D. Kim, H. S. Choi, J. C. Park, Y. S. Nam and D. Y. Jeon, *RSC Adv.*, 2017, **7**, 10675–10682.
29. A. C. Berends, F. T. Rabouw, F. C. M. Spoor, E. Bladt, F. C. Grozema, A. J. Houtepen, L. D. A. Siebbeles and C. De Mello Donegá, *J. Phys. Chem. Lett.*, 2016, **7**, 3503–3509.
30. L. Li, A. Pandey, D. J. Werder, B. P. Khanal, J. M. Pietryga and V. I. Klimov, *J. Am. Chem. Soc.*, 2011, **133**, 1176–1179.
31. R. Xie, M. Rutherford and X. Peng, *J. Am. Chem. Soc.*, 2009, **131**, 5691–5697.
32. H. Zang, H. Li, N. S. Makarov, K. A. Velizhanin, K. Wu, Y. S. Park and V. I. Klimov, *Nano Lett.*, 2017, **17**, 1787–1795.
33. C. Xia, J. D. Meeldijk, H. C. Gerritsen and C. De Mello Donega, *Chem. Mater.*, 2017, **29**, 4940–4951.
34. A. D. P. Leach, L. G. Mast, E. A. Hernández-Pagán and J. E. Macdonald, *J. Mater. Chem. C*, 2015, **3**, 3258–3265.
35. A. D. P. Leach, X. Shen, A. Faust, M. C. Cleveland, A. D. La Croix, U. Banin, S. T. Pantelides and J. E. Macdonald, *J. Phys. Chem. C*, 2016, **120**, 5207–5212.
36. S. L. Castro, S. G. Bailey, R. P. Raffaelle, K. K. Banger and A. F. Hepp, *J. Phys. Chem. B*, 2004, **108**, 12429–12435.
37. S. K. Batabyal, L. Tian, N. Venkatram, W. Ji and J. J. Vittal, *J. Phys. Chem.*, 2009, **113**, 15037–15042.
38. C. Sun, Z. Cevher, J. Zhang, B. Gao, K. Shum and Y. Ren, *J. Mater. Chem. A*, 2014, **2**, 10629.
39. C. Fradler, T. Rath, S. Dunst, I. Letofsky-Papst, R. Saf, B. Kunert, F. Hofer, R. Resel and G. Trimmel, *Sol. Energy Mater. Sol. Cells*, 2014, **124**, 117–125.
40. C. Buchmaier, T. Rath, F. Pirolt, A.-C. Knall, P. Kaschnitz, O. Glatter, K. Wewerka, F. Hofer, B. Kunert, K. Krenn and G. Trimmel, *RSC Adv.*, 2016, **6**, 106120–106129.
41. D. P. Dutta and G. Sharma, *Mater. Lett.*, 2006, **60**, 2395–2398.
42. S. Ghoshal, A. Wadawale and V. K. Jain, *Anal. Sci. X-ray Struct. Anal. Online*, 2008, **24**, x15–x16.
43. Y. Qi, Q. Liu, K. Tang, Z. Liang, Z. Ren and X. Liu, *J. Phys.*

Chem. C, 2009, **113**, 3939–3944.
44. D. Pan, L. An, Z. Sun, W. Hou, Y. Yang, Z. Yang and Y. Lu, *J. Am. Chem. Soc.*, 2008, **130**, 5620–5621.
45. G. B. Shombe, E. B. Mubofu, S. Mlowe and N. Revaprasadu, *Mater. Sci. Semicond. Process.*, 2016, **43**, 230–237.
46. E. B. Mubofu, *Sustain. Chem Process*, 2016, **4**, 11.
47. S. C. Masikane and N. Revaprasadu, *Mater. Sci. Semicond. Process.*, 2018, **76**, 73–79.
48. S. Mourdikoudis and L. M. Liz-Marzán, *Chem. Mater.*, 2013, **25**, 1465–1476.
49. S. Lei, C. Wang, L. Liu, D. Guo, C. Wang, Q. Tang, B. Cheng, Y. Xiao and L. Zhou, *Chem. Mater.*, 2013, **25**, 2991–2997.
50. J. Ạlvarez-García, A. Pérez-Rodríguez, B. Barcones, A. Romano-Rodríguez, J. R. Morante, A. Janotti, S.-H. Wei and R. Scheer, *Appl. Phys. Lett.*, 2002, **80**, 562–564.
51. D. Y. Lee and J. Kim, *Thin Solid Films*, 2010, **518**, 6537–6541.
52. J. Álvarez-García, J. Marcos-Ruzafa, A. Pérez-Rodríguez, A. Romano-Rodríguez, J. R. Morante and R. Scheer, *Thin Solid Films*, 2000, **361**, 208–212.
53. S. Y. Lee and B. O. Park, *Thin Solid Films*, 2008, **516**, 3862–3864.
54. M. G. Panthani, V. Akhavan, B. Goodfellow, J. P. Schmidtke, L. Dunn, A. Dodabalapur, P. F. Barbara and B. A. Korgel, *J. Am. Chem. Soc.*, 2008, **130**, 16770–16777.
55. A. M. Hounslow and E. R. T. Tiekink, *J. Crystallogr. Spectrosc. Res.*, 1991, **21**, 133–137.

Journal Name

ARTICLE

On the Phase Control of $CuInS_2$ Nanoparticles from Cu-/In-Xanthates

Mundher Al-Shakban,[a] Peter D Matthews,[b,c] Xiang L. Zhong,[a] Inigo Vitorica-Yrezabal,[b] James Raftery,[b] Daivd J. Lewis[a] and Paul O'Brien*[a,b]